

NONLINEAR OPTICAL PHENOMENA

PACS numbers: 42.50.Gy
DOI: 10.1070/QE2014v044n02ABEH015277

Numerical simulation of adiabatons in electromagnetically induced transparency under quasi-resonance conditions

O.M. Parshkov, E.R. Govorenko

Abstract. **The evolution of adiabatons in electromagnetically induced transparency in the Λ scheme of degenerate quantum transitions J = 0 → J = 1 → J = 2 with Doppler broadening of spectral lines has been numerically simulated taking into account the effect of resonance detunings. It is shown that, in the case of linearly polarised fields, an increase in the probe-field resonance detuning (under exact-resonance conditions for the control radiation) leads to a transformation of electromagnetically induced transparency into electromagnetically induced absorption at certain stages. When the control-field resonance detuning is varied, the transparency of the medium for the probe (exactly resonant) radiation monotonically decreases with increasing detuning because of the rising role of single-photon absorption. In the case of circularly polarised control radiation and linearly polarised input probe field, a probe pulse propagating in the medium splits into two pulses with oppositely directed circular polarisations. An increase in the probe pulse resonance detuning (under exact-resonance conditions for the control radiation) leads primarily to an increase in the absorption by the medium of the probe pulse, the direction of circular polarisation for which coincides with the circular-polarisation direction for the control radiation.**

Keywords: *electromagnetically induced transparency, adiabaton, inhomogeneous broadening, degeneracy of levels, resonance detuning.*

1. Introduction

Electromagnetically induced transparency (EIT) [1] is one of most important quantum interference effects in laser physics. Intensive study of EIT has led to significant progress in the development of quantum storage [2] and quantum communication [2–4] systems, the theory of quantum information [1, 2, 5], the design of systems for exact magnetic measurements [6], and in chronometry [7]. In addition, EIT is efficiently used to form large optical nonlinearities [5, 8]. To date, this effect is observed not only in atomic and molecular systems but also in solids with rare earth impurities [9], semiconductors with quantum wells [10], superconducting structures [11], and metamaterials [12]. Another important and widely studied quantum interference effect is electromagnetically induced absorption [13, 14], which is in essence opposite to EIT.

Adiabaton is a pulsed EIT pair. It is composed of a probe-radiation pulse and a dip in the flat top of a control field pulse, which propagate jointly and without distortions through a medium. The first theory of adiabaton was reported in [15–17]; then it was refined in [18, 19]. In these studies, the quantum-transition levels were considered as nondegenerate, and the frequencies of the probe and control fields were assumed to be equal to the frequencies of the corresponding resonant transitions; the inhomogeneous broadening of spectral lines was disregarded.

In this paper, we report the results of numerical analysis of the influence of resonance detunings of probe and control pulses on the adiabaton parameters. An increase in the aforementioned detunings is expected to lead, on the one hand, to an increase in attenuation of the adiabaton probe component in the medium because of the deviation from the adiabatic-following conditions [20, 21] and, on the other hand, to reduction of this attenuation because of the decrease in the single-photon absorption efficiency. The purpose of our study was to determine the result of the competition of these tendencies. We did not use the adiabatic-following approximation (characteristic of [15–19]) as a start point; however, the calculation parameters were chosen so as to make approximation applicable in principle. The calculations were performed for the Λ scheme of inhomogeneously broadened quantum transitions between the degenerate energy levels $^3P_0$, $^3P_2$ and $^3P_1^0$ of the ^{208}Pb isotope, in vapour of which EIT of circularly polarised laser fields was observed [22].

2. Statement of the problem

Let us consider a Λ scheme including a nondegenerate lower level (J = 0), a fivefold degenerate intermediate level (J = 2), and a triply degenerate upper level (J = 1), formed by the $^3P_0$, $^3P_2$, and $^3P_1^0$ levels of the ^{208}Pb isotope. Let ϕ_k ($k = 1, 2, \ldots, 9$) be an orthonormal set of common eigenfunctions of Hamilton operators, the angular momentum, and its component in the z axis for an isolated atom, which correspond to the lower ($k = 1$, $M = 0$), upper ($k = 2, 3, 4$, $M = 1, 0, 1$, respectively), and intermediate ($k = 5, 6, \ldots, 9$, $M = -2, -1, 0, 1, 2$, respectively) levels. Let D_1 and D_2 be reduced electric dipole moments of the J = 0 → J = 1 and J = 2 → J = 1 transitions, respectively, and ω_{10} and ω_{21} be the frequencies of these transitions for an atom at rest. We assume also that $T_1 = 1/\Delta_1$, where Δ_1 is the half-width at the level of e^{-1} height of the density distribution of the frequencies ω'_{10} of the J = 0 → J = 1 quantum transitions as a result of the Doppler effect.

O.M. Parshkov, E.R. Govorenko Yuri Gagarin State Technical University of Saratov, Politekhnicheskaya ul. 77, 410054 Saratov, Russia; e-mail: oparshkov@mail.ru, ekaterinagovorenko@gmail.com

Received 12 July 2013; revision received 20 September 2013
Kvantovaya Elektronika **44** (2) 122–129 (2014)
Translated by Yu.P. Sin'kov

The electric field of two laser pulses with carrier frequencies ω_1 and ω_2 (the probe and control pulses, respectively; $\omega_1 > \omega_2$), propagating along the z axis, can be presented in the form

$$\boldsymbol{E} = \mathrm{Re}\sum_{l=1}^{2}\mu_l(\boldsymbol{e}_+ f_l + \boldsymbol{e}_- g_l)\exp[\mathrm{i}(\omega_l t - k_l z)], \quad (1)$$

where $\mu_l = \hbar\sqrt{2l+1}\,(|D_1|T_1)^{-1}$; $\boldsymbol{e}_+ = \boldsymbol{e}_-^* = (\boldsymbol{i} + \mathrm{i}\boldsymbol{j})/2$; $\boldsymbol{i}, \boldsymbol{j}$ are the unit vectors of the x and y axes, respectively; f_l and g_l are the complex amplitudes of the right- and left-handed circularly polarised components of the probe ($l = 1$) and control ($l = 2$) fields, which are functions of z and t; and $k_l = \omega_l/c$. When studying the case of quasi-resonance, we suggest that the differences between the frequencies ω_{10} and ω_1, as well as between the frequencies ω_{21} and ω_2, are much smaller than these frequencies. The ε_{10} and ε_{20} values, which are called below the resonance detunings of the probe and control fields, respectively, are determined by the formulas

$$\varepsilon_{10} = (\omega_{10} - \omega_1)/\Delta_1,\ \varepsilon_{20} = (\omega_{21} - \omega_2)/\Delta_1, \quad (2)$$

they play the role of dimensionless parameters specifying the measure of this difference.

The atomic wave function can be presented as

$$\Psi = \bar{c}_1\phi_1 + \left(\sum_{k=2}^{4}\bar{c}_k\phi_k\right)\exp(-\mathrm{i}\xi_1) + \left(\sum_{k=5}^{9}\bar{c}_k\phi_k\right)\exp[-\mathrm{i}(\xi_1 - \xi_2)],$$

where $\xi_l = \omega_l t - k_l z$; $l = 1, 2$. Let us introduce quantities c_i,

$$c_1 = p_1^*\bar{c}_1,\ c_2 = \bar{c}_2,\ c_4 = \bar{c}_4,\ c_5 = p_2\bar{c}_5,\ c_7 = (1/\sqrt{6})p_2\bar{c}_7,\ c_9 = p_2\bar{c}_9,$$

where $p_l = 2D_l/|D_l|$; $l = 1, 2$. Then, we will determine the normalised independent variables s and w as

$$s = z/z_0,\ w = (t - z/c)/T_1, \quad (3)$$

where $z_0 = 3\hbar c/(2\pi N|D_1|^2 T_1\omega_1)$, and N is the atomic concentration. Using the Maxwell and Schrödinger equations, we obtain the following system of equations in the approximation of slowly varying amplitudes:

$$\frac{\partial f_1}{\partial s} = \frac{\mathrm{i}}{\sqrt{\pi}}\int_{-\infty}^{+\infty} c_1 c_2^* \exp[-(\varepsilon_1 - \varepsilon_{10})^2]\,\mathrm{d}\varepsilon_1,$$

$$\frac{\partial f_2}{\partial s} = -\frac{\mathrm{i}}{\sqrt{\pi}}\xi\int_{-\infty}^{+\infty}(c_4^* c_9 + c_2^* c_7)\exp[-(\varepsilon_1 - \varepsilon_{10})^2]\,\mathrm{d}\varepsilon_1,$$

$$\frac{\partial g_1}{\partial s} = -\frac{\mathrm{i}}{\sqrt{\pi}}\int_{-\infty}^{+\infty} c_1 c_4^* \exp[-(\varepsilon_1 - \varepsilon_{10})^2]\,\mathrm{d}\varepsilon_1,$$

$$\frac{\partial g_2}{\partial s} = \frac{\mathrm{i}}{\sqrt{\pi}}\xi\int_{-\infty}^{+\infty}(c_2^* c_5 + c_4^* c_7)\exp[-(\varepsilon_1 - \varepsilon_{10})^2]\,\mathrm{d}\varepsilon_1,$$

$$\frac{\partial c_1}{\partial w} = -\mathrm{i}(f_1 c_2 - g_1 c_4), \quad (4)$$

$$\frac{\partial c_2}{\partial w} + \mathrm{i}\varepsilon_1 c_2 = -\frac{\mathrm{i}}{4}(f_1^* c_1 + g_2^* c_5 - f_2^* c_7) - \gamma c_2,$$

$$\frac{\partial c_4}{\partial w} + \mathrm{i}\varepsilon_1 c_4 = \frac{\mathrm{i}}{4}(g_1^* c_1 - g_2^* c_7 + f_2^* c_9) - \gamma c_4,$$

$$\frac{\partial c_5}{\partial w} + \mathrm{i}(\varepsilon_1 - \varepsilon_2)c_5 = -\mathrm{i}g_2 c_2,$$

$$\frac{\partial c_7}{\partial w} + \mathrm{i}(\varepsilon_1 - \varepsilon_2)c_7 = \frac{\mathrm{i}}{6}(f_2 c_2 - g_2 c_4),$$

$$\frac{\partial c_9}{\partial w} + \mathrm{i}(\varepsilon_1 - \varepsilon_2)c_9 = -\mathrm{i}f_2 c_4,$$

where

$$\varepsilon_1 = (\omega'_{10} - \omega_1)/\Delta_1;\ \varepsilon_2 = \varepsilon_{20} + \frac{\omega_{21}}{\omega_{10}}(\varepsilon_1 - \varepsilon_{10}); \quad (5)$$

$$\xi = 0.75\frac{\omega_{21}}{\omega_{10}}|D_2/D_1|^2.$$

In view of the selection rules ($\Delta M = \pm 1$) for the transitions under the action of circularly polarised field components (1), the amplitudes $\bar{c}_3$, $\bar{c}_6$, and $\bar{c}_8$ do not enter system (4). The energy diagram for the states that can be involved in the interaction of waves is shown in Fig. 1. The consideration of the Doppler broadening of quantum-transition lines via averaging of the field-induced dipole moments of individual atoms over the parameter ε_1, which is unambiguously related to the thermal velocity of each atom along the z axis, gave rise to integrals in the first four equations of system (4) and to a peculiar relationship between ε_1 and ε_2 (here, $\varepsilon_2 = (\omega'_{21} - \omega_2)/\Delta_1$, where ω'_{21} is the frequency of the J = 2 → J = 1 quantum transition in a moving atom.)

States 2 and 4 of the ^{208}Pb isotope are subjected to spontaneous decay with a transition to the other states of the Λ scheme under consideration (states 1, 5, 7, and 9) and to the states that are not covered by the Λ scheme. The latter include states 6 and 8 of the intermediate energy level, as well as states

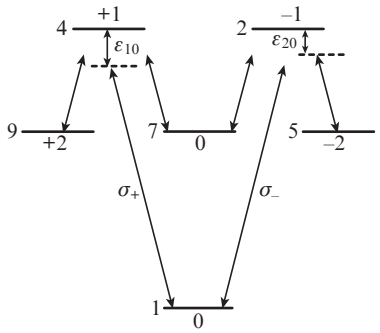

Figure 1. Schematic diagram of quantum transitions. The numbers on the left from the horizontal lines enumerate states, and the numbers from above or below are the quantum numbers M of the states. The arrows inclined to the left (to the right) indicate transitions induced by the σ_+ (σ_-) field components.

located below the $^3P_1$ level. Estimates based on the oscillator strengths of the ^{208}Pb isotope [23] show that the probability of the spontaneous transition from each of the upper states of the Λ scheme (states 2 and 4) to the states that do not enter this scheme is approximately equal to the spontaneous transition probability to all lower states included in the Λ scheme. We assume for simplification that the lifetime of each from states 2 and 4 with respect to the spontaneous decay is determined by only the transition to the states that do not enter the Λ scheme. To take into consideration this spontaneous decay, we phenomenologically introduced relaxation terms $-\gamma c_2$ and $-\gamma c_4$ into the equations for c_2 and c_4. Here, $\gamma = T_1/(2\tau)$ (τ is the radiative lifetime of the $^3P_1^0$ level). According to [23], $\omega_{21}/\omega_{10} = 0.7$, $\xi = 2.11$, and (at $T = 900-1000$ K) $\gamma = 1.5\times10^{-2}$ for the chosen transitions in ^{208}Pb.

Below we use the parameters a_l, α_l, and γ_l for the polarisation ellipse of the probe ($l = 1$) and control ($l = 2$) pulses. Here, a_l is the semimajor axis of the ellipse (measured in μ_l units), α_l is its tilt angle with respect to the x axis, and γ_l is the contraction ratio ($a_l \geqslant 0$, $0 \leqslant \alpha_l < \pi$, $-1 \leqslant \gamma_l \leqslant +1$ [24]). The $|\gamma_l|$ value is the ratio of the minor axis of ellipse to its major axis. The condition $0 < \gamma_l < +1$ ($-1 < \gamma_l < 0$) corresponds to the right-handed (left-handed) elliptical polarisation; $\gamma_l = 0$ indicates linear polarisation; and, at $\gamma_l = 1$ and -1, we have right-handed circular polarisation (σ_- polarisation) and left-handed circular polarisation (σ_+ polarisation). When $|\gamma_l| = 1$, the angle α_l is not determined and is formally assumed to be -0.1.

The initial conditions for system (4) correspond to the situation where all atoms occupy the lower energy level at the initial instant ($w = 0$). The boundary conditions, which describe the probe radiation at the input ($s = 0$) of the resonant medium, were chosen in the form

$$\alpha_1 = 0.5,\ a_1 = 0.22\,\mathrm{sech}[(w - 170)/38],\ \gamma_1 = 0, \qquad (6)$$

and the input field of the control radiation was set by the relations

$$\alpha_2 = \alpha_{20},\ a_2 = a_{20}\{\mathrm{th}[(w - 30)/10] + 1\},\ \gamma_2 = \gamma_{20}, \qquad (7)$$

where α_{20}, a_{20}, and γ_{20} are constants.

Equalities (6) describe the input bell-shaped pulse of probe radiation, the FWHM of which is about 70 (on the time scale w). This pulse is linearly polarised, with a polarisation direction making an angle of about 30° with respect to the x axis. Equality (7) describes the field of the control radiation incident on the input surface of the resonant medium so that its intensity remains constant while the probe pulse intersects this surface. The parameter a_{20} determines the field strength for the flat top of the input control pulse; its value is chosen so as to exceed the peak field strength of the input probe pulse by a factor of about 20.

The calculation results are presented in terms of intensities I_l ($l = 1, 2$), i.e., the energy flux densities of the probe ($l = 1$) and control ($l = 2$) fields, measured in $c\mu_1^2/(8\pi)$ units. The transmittance Tr, which characterises the transparency of the medium for the probe radiation, is given by the formula $\mathrm{Tr} = W_1(s)/W_1(0)$, where $W_1(0)$ and $W_1(s)$ are, respectively, the energies (per cross-sectional area unit) of the probe pulse at the resonant-medium input and at a distance of s in the medium bulk.

3. Calculation results

(1) Let us consider the case of fields of probe and control pulses linearly polarised in the same direction by assuming that $\alpha_{20} = 0.5$, $a_{20} = 3.5$, and $\gamma_{20} = 0$ in (7). Under these conditions, each pulse has circular σ_+ and σ_- components of equal intensity, which provide transitions between all states shown in Fig. 1. Here, the variable parameter is ε_{10} (probe-field resonance detuning), while the control-radiation resonance detuning is absent ($\varepsilon_{20} = 0$).

The solid lines in Fig. 2 are the dependences of the probe pulse intensities on w at several fixed distances s for $\varepsilon_{10} = 0$, 1.2, and 7. According to Fig. 2, the transparency of the medium for the probe radiation is the highest for an exactly resonant probe field [$\varepsilon_{10} = 0$, curve (*1*) in Figs 2b–2d], which is in good agreement with the general concepts of the EIT theory [1]. With an increase in ε_{10}, the probe-pulse absorption first increases and then decreases, as follows from the comparison of curves (*2*) ($\varepsilon_{10} = 1.2$) and (*3*) ($\varepsilon_{10} = 7$) in Figs 2b–2d.

Figure 3 shows the dependence of the transmittance Tr of probe radiation on ε_{10} ($\varepsilon_{10} \geqslant 0$) for the distances $s = 10$, 100, and 500, in the presence of control radiation [curves (*1*), (*2*), and (*3*), respectively] and in its absence [curves (*1′*), (*2′*), and (*3′*), calculated for $a_{20} = 0$]. Note that Tr is an even function of the argument ε_{10} in this case. According to Fig. 3, the transmittance Tr is maximum and practically complete (Tr = 1) for all distances s at $\varepsilon_{10} = 0$ (i.e., when the exact-resonance conditions are satisfied for both interacting pulses). With an increase in $|\varepsilon_{10}|$, the transmittance decreases almost to zero and the transmittance curves near the point $\varepsilon_{10} = 0$ are bell-shaped [see curves (*1–3*) in the range $\varepsilon_{10} < 2$ in Fig. 3]. The FWHM of the transmission band found from these curves decreases with an increase in the distance s and amounts to $4.4\Delta_1$, $3.2\Delta_1$ and $2.4\Delta_1$ for $s = 10$, 100 and 500, respectively. In other words, the transmission bandwidth is approximately one to two Doppler widths of the $J = 0 \to J = 1$ transition, which is resonant with the probe field. As curves (*1–3*) indicate, the transmittance monotonically increases at sufficiently large ε_{10} values ($\varepsilon_{10} > 3-4$). The dependences of Tr on ε_{10} exhibit dips with a width of few Δ_1 values.

A comparison of the curves in Fig. 3 shows that the region that is characterised by almost complete absorption of probe radiation in the presence of the control field exhibits a significant transmittance of the probe pulse in the absence of the control field. Moreover, beyond the absorption range, from the side of large ε_{10} values (the range $\varepsilon_{10} > 3-4$ in Fig. 3), the probe-pulse transmittance in the presence of control radiation remains smaller than without it. These facts can be interpreted as a transition from EIT to electromagnetically induced absorption with an increase in the absolute value of the detuning ε_{10}.

The width of the central transmittance peak, where EIT plays a key role in the adiabaton evolution, and the range of resonance detuning, where absorption dominates, exceed the Doppler width of the inhomogeneously broadened profile of the $J = 0 \to J = 1$ transition. This circumstance is explained (see, for example, [5]) by the choice of such a high control field strength in our calculation that the Rabi frequency of each its circular component exceeds Δ_1 by a factor of about 5. Note that, at fairly low Rabi frequencies of the control field, both EIT and absorption manifest themselves in the form of resonances, which are much narrower than the Doppler (or even uniform) profiles of spectral lines [1, 13, 14].

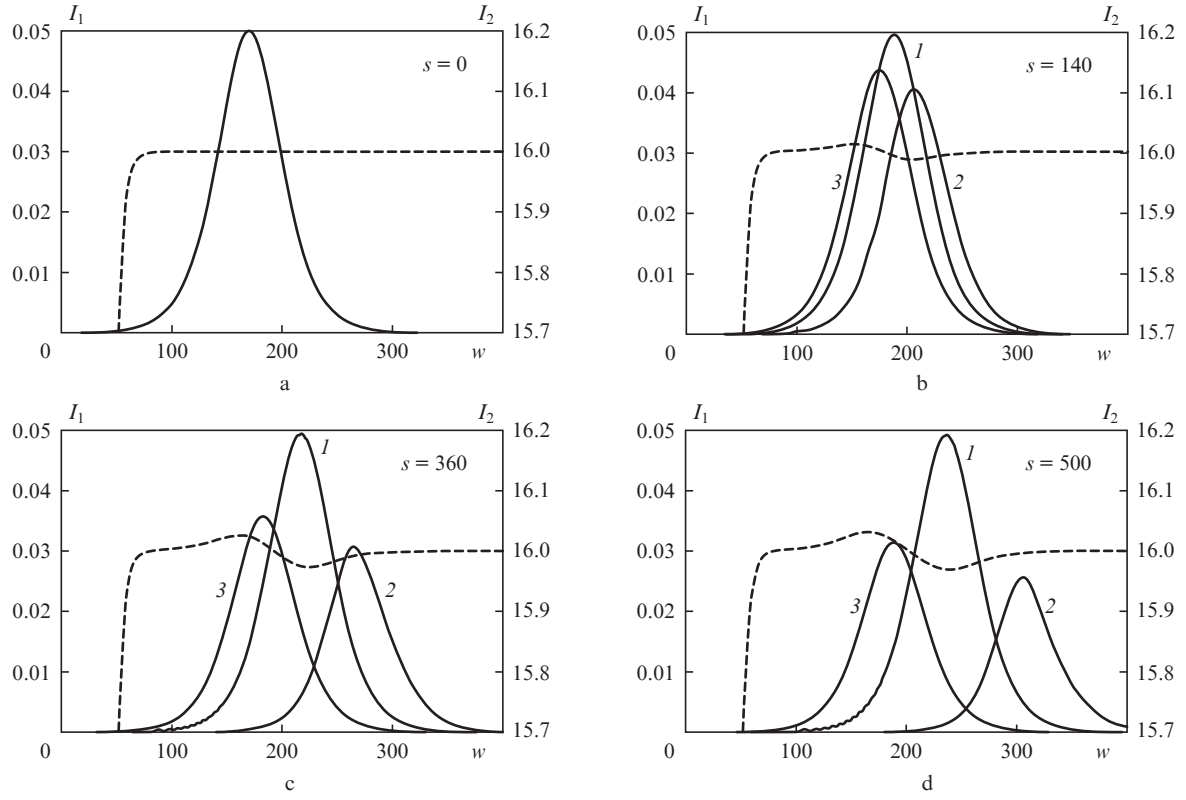

Figure 2. Evolution of the intensity I_1 of the adiabaton probe component at different s values and $\varepsilon_{10} = (1)\ 0, (2)\ 1.2$, and $(3)\ 7$ and the control-field intensity I_2 at $\varepsilon_{10} = 0$ (dashed lines).

Figure 4 shows the dependence of the c/c_1 ratio on ε_{10} (c is the speed of light in vacuum and c_1 is the average probe-pulse velocity in the medium for a specified distance s, which is determined as the displacement velocity of the point of maximum intensity). The c/c_1 value depends strongly on the concentration N of active-medium vapour. When plotting Fig. 4, it was assumed that $N = 3.4\times10^{13}$ cm^{-3}, which corresponds to the concentration of saturated lead vapour at $T = 950$ K (the details of choosing the numerical values of the parameters of the medium are presented in Section 4). The c/c_1 ratio was determined for $s = 30$ and 100. At $\varepsilon_{10} \sim 2$–4 the probe radiation is completely absorbed at these distances; therefore, the dependences of c/c_1 on ε_{10} are omitted for this range.

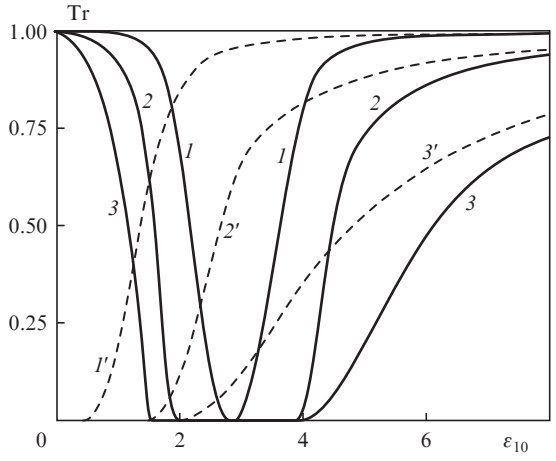

Figure 3. Dependences of the transmittance Tr of the adiabaton probe pulse on ε_{10} at s = 10, 100, and 500 in the presence of a control field [curves (*1*), (*2*), and (*3*), respectively] and in its absence [(*1′*), (*2′*), and (*3′*), respectively].

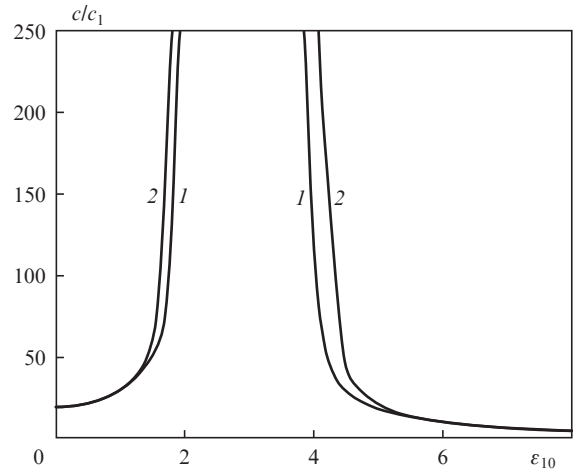

Figure 4. Dependences of the c/c_1 ratio on ε_{10} at $s = (1)\ 30$ and $(2)\ 100$.

The discrepancy between curves (*1*) and (*2*) indicates that the instantaneous pulse velocity is not a constant. At $\varepsilon_{10} = 0$ (case of exact resonance) $c/c_1 \cong 19$ for both distances, and near the points $\varepsilon_{10} = 2$ and 4 the c/c_1 value is larger by a factor of about 13. At large ε_{10} detunings ($\varepsilon_{10} > 4$, see Fig. 4), the c/c_1 ratio monotonically decreases, reaching ~4 at $\varepsilon_{10} = 8$. Thus,

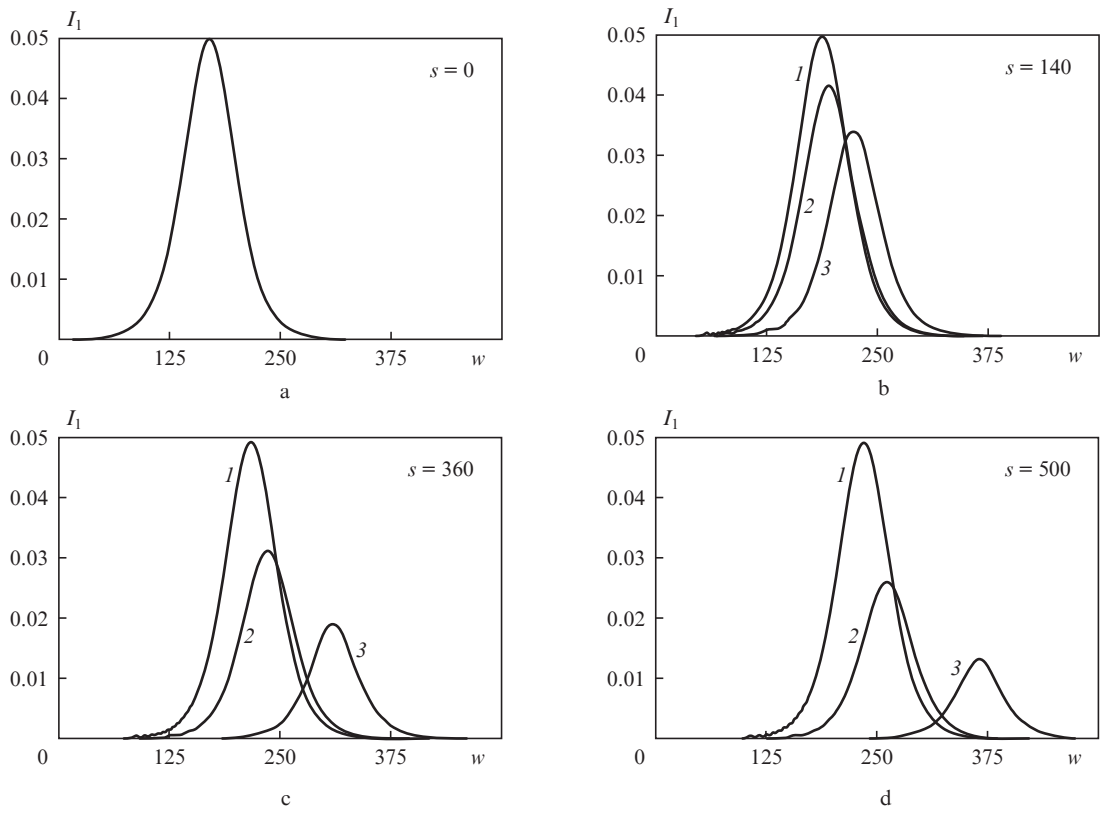

Figure 5. Evolution of the intensity I_1 of the adiabaton probe component at different s and $\varepsilon_{20} = (1)\ 0, (2)\ 1.5$, and $(3)\ 2.5$.

the velocity of the adiabaton probe pulse depends strongly on the detuning ε_{10}.

An analysis of the complex amplitudes f_1 and g_1 of the right- and left-handed circularly polarised components of the probe field showed that their phases are independent of the variable w. This means that during propagation of a probe pulse its instantaneous frequency ω_1 remains constant and equal to its value at the input of the resonant medium. However, the phases of these amplitudes linearly depend on the variable s. For example, at $\varepsilon_{10} = 0.5$ and $s = 45$, the complex-amplitude phases increase by π.

The dashed curves in Fig. 2 are the dependences of the control-field intensity on w for several distances s in the case of $\varepsilon_{10} = 0$ (the scale for these curves is smaller than the scale for the dependences of the probe-field intensities by a factor of 10). It can be seen that a characteristic 'hump' arises in the flat top of the control pulse, which propagates with a speed of light in vacuum, and that there is a dip in the region of the probe pulse. This control-field structure, which is characteristic of EIT adiabatons [15–18], is also observed for other resonance detunings ε_{10} considered in our calculations.

(2) The α_{20}, a_{20}, and γ_{20} values are retained, but now the control-field resonance detuning ε_{20} is varied, whereas the probe-pulse resonance detuning is absent ($\varepsilon_{10} = 0$). Figure 5 shows the dependence of the probe pulse intensities on w at several fixed distances s for $\varepsilon_{20} = 0$, 1.5, and 2.5.

Figure 6 shows the dependences of the probe-radiation transmittance Tr on ε_{20} ($\varepsilon_{20} \geqslant 0$) for $s = 10$, 100, and 500 (Tr is an even function of detuning ε_{20}.) As follows from the shape of the curves in Figs 5 and 6, an increase in $|\varepsilon_{20}|$ leads to a monotonic decrease in the probe-pulse transmittance. This effect is related to the decrease in the EIT efficiency with an increase in the control-field resonance detuning [5]. Under these conditions, the probe-pulse propagation velocity monotonically decreases. With the same values of the resonant-medium parameters, which were used above to estimate the c/c_1 ratio, we found that the probe pulse velocity at $\varepsilon_{20} = 2.5$ [Fig. 5, curve (3)] is smaller than that at $\varepsilon_{20} = 0$ [Fig. 5, curve (1)] by a factor of 3.

Since dependences of the control-field intensity I_2 on w at fixed distances s are similar to the corresponding curves calculated in Section 1, they are omitted here.

(3) Let us assume that $\alpha_{20} = -0.1$, $a_{20} = 2.46$, and $\gamma_{20} = -1$ in (7). This situation corresponds to the case of σ_+ (left-handed circular) polarisation of the input control radiation

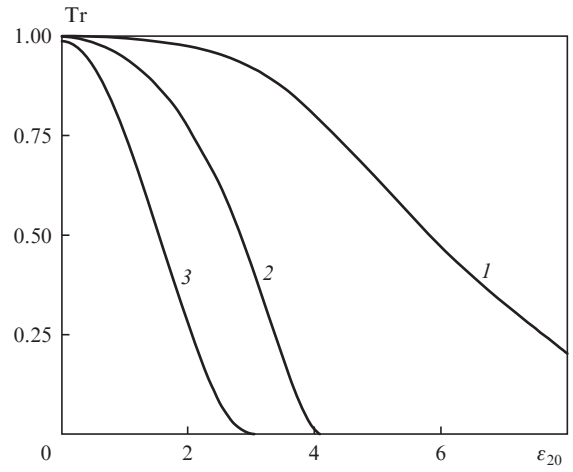

Figure 6. Dependences of the transmittance Tr of the adiabaton probe pulse on ε_{20} at $s = (1)\ 10, (2)\ 100$, and $(3)\ 500$.

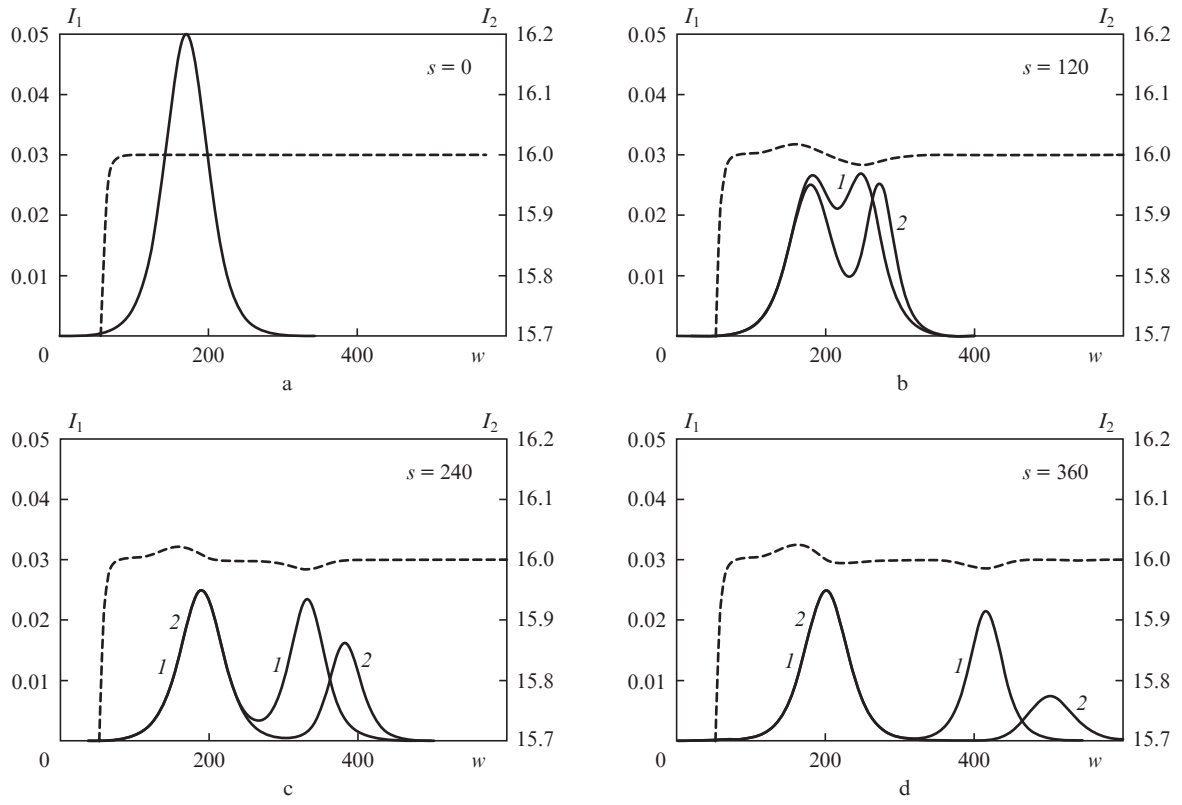

Figure 7. Evolution of the intensity I_1 of the adiabaton probe component at different s for ε_{10} = (*1*) 0 and (*2*) 0.2 and the control-field intensity I_2 at $\varepsilon_{10} = 0$ (dashed lines).

with the same height of the flat top as in the calculations performed in Sections 1 and 2. Here, the variable parameter is the resonance detuning ε_{10} for the probe-field frequency, whereas the control field is assumed to be exactly resonant ($\varepsilon_{20} = 0$).

The solid curves in Fig. 7 are dependences of the probe-pulse intensity on w at several fixed distances s for $\varepsilon_{10} = 0$ and 0.2. According to the calculations for both detunings, the probe-radiation pulse is split into two individual pulses during its propagation through the medium (Figs 7b–7d). A similar splitting was found and described in detail in [25]; therefore, we will only briefly dwell on its physical nature.

The linearly polarised field of the input probe pulse is a superposition of circular σ_+ and σ_- components, whereas the input control field contains only a σ_+ component. As a result, one can select two Λ schemes from the Λ scheme of degenerate levels (see Fig. 1) by excluding the short right-inclined arrows from it. The σ_+ component of the probe field evolves in the Λ scheme composed of states 1, 4, and 7, while the σ_- component evolves in the Λ scheme containing states 1, 2, and 5. Each circular component of the input probe radiation generates its own probe pulse with the same polarisation in the medium. In view of the difference in the propagation velocities of these pulses, the input probe pulse splits into two pulses; note that the σ_- component of the probe field has a higher intensity. This consideration is confirmed by the data in Fig. 8, which presents the dependences of I_1 and γ_1 on w at $s = 360$ and $\varepsilon_{10} = 0.2$. The shape of the curve describing the evolution of γ_1 suggests that $\gamma_1 = 1$ (σ_- polarisation) in the localisation region of the first pulse of the probe field, whereas in the second-pulse localisation region $\gamma_1 = -1$ (σ_+ polarisation).

The coincidence of curves *1* and *2* in the region of the probe pulse with σ_- polarisation (the probe pulse with left-handed polarisation in Figs 7c and 7d) indicates that, in the case of small detuning ε_{10}, a probe pulse with this polarisation barely differs from the corresponding pulse under exact-resonance conditions ($\varepsilon_{10} = 0$). However, the evolution of σ_+-polarised probe pulses with such a change in detuning ε_{10} is significantly different: at $\varepsilon_{10} = 0.2$, the damping of this probe-radiation component is much larger, while the propagation velocity is smaller than at $\varepsilon_{10} = 0$. At $\varepsilon_{10} > 1$, as additional calculations showed, the σ_+ component of the probe

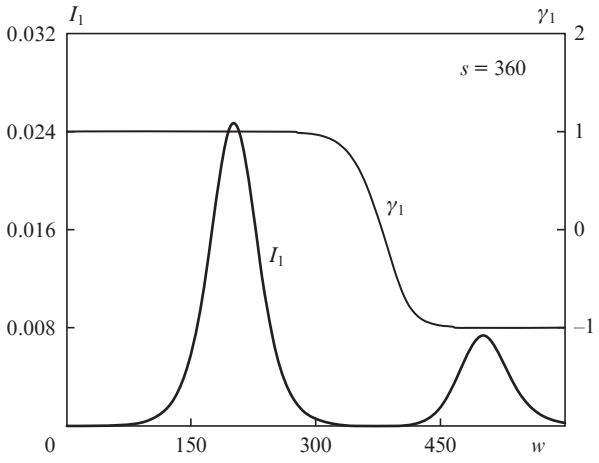

Figure 8. Dependences of the intensity I_1 and the polarisation-ellipse contraction ratio γ_1 for the probe radiation on w at $\varepsilon_{10} = 0.2$ and $s = 360$.

field is absorbed by the medium at a distance $s < 10$. At larger distances, only the σ_--polarised probe pulse remains in the medium. This fact can be interpreted as the control-field-induced circular dichroism [26] for the probe field.

The dashed curves in Fig. 7 are the dependences of the control-field intensity at $\varepsilon_{10} = 0$. One can see (Figs 7c and 7d) that a 'hump' arises in the control-pulse top, which is followed by two dips above each probe pulse.

A change in the sign of detuning $\varepsilon_{10} = 0$ does not change the shape of the curves presented in Figs 7 and 8. If the input control field is σ_--polarised, one should replace σ_- with σ_+ and vice versa where necessary and invert the curve γ_1 (thin line in Fig. 8) with respect to the abscissa axis. Note that the calculations in Sections 1 and 2 were performed without changing the polarisation state of the fields propagating in the medium.

4. Dimensional estimates

The concentration of ^{208}Pb-isotope vapour N is an important parameter for estimating the possibility of experimental verification of the theoretical conclusions. Another important parameter of the theory is the inhomogeneous-broadening 'time' T_1. These values enter the normalisation conditions (3). In the case of saturated vapour, N and T_1 are interrelated through the absolute temperature T.

For the temperature $T = 950$ K, according to [27], $N = 3.4\times10^{13}$ cm^{-3} and $T_1 = 1.63\times10^{-10}$ s for saturated ^{208}Pb vapour.

Using the data of [23] on the oscillator strengths of quantum transitions, we find that $z_0 = 0.03$ cm. Note that at this distance the probe-pulse energy W_1 in the absence of control field decreases by a factor of about 20. The width of the input probe pulse ($s = 0$) is about 10 ns (at half maximum of the intensity envelope I_1).

The intensities of the probe and control fields ($\bar{I}_1$ and $\bar{I}_2$, respectively) in the range of absolute temperatures from 900 to 1000 K can be estimated in kW cm^{-2} from the formula $\bar{I}_l = 1.3I_l$, $l = 1, 2$. In particular, the above calculations showed that the peak intensity of the input probe pulse is ~65 W cm^{-2} and the intensity corresponding to the flat top of the input control-field pulse is ~20 kW cm^{-2}.

Our simplified procedure for taking into account the relaxation processes ignores the fact that the spontaneous decay of states 2 and 4 of the ^{208}Pb isotope involves not only transitions beyond the scheme under study (i.e., the external transitions) but also the transitions to the states of the Λ scheme (states 1, 5, 7, 9; internal transitions). This way for taking into account relaxation in the case under consideration can be substantiated as follows. The resulting effect of each relaxation decay of states 2 and 4 is reduced to a decrease in the probe energy. The difference of external spontaneous transitions from internal ones is that the former transfer the atom from the state of interaction with the radiation field, whereas the internal transitions allow the atom to be involved in this interaction even after they are finished. However, according to [23], the radiative lifetime of states 2 and 4 is 17 ns, whereas the pulse width obtained in our calculations is close to 10 ns. Since the probe-pulse duration is shorter than the radiative lifetime of states 2 and 4, an internal spontaneous transition occurs after the probe pulse leaves the localization region of atom. This means that the atoms undergoing an internal spontaneous transition are also transferred from the state of interaction with the radiation field. Therefore, the internal transitions can be taken into account by including them in the number of external transitions.

5. Conclusions

We presented the results of the calculations modelling the influence of detunings of the probe and control frequencies from the central frequencies of the corresponding inhomogeneously broadened quantum transitions on the evolution of adiabatons. It was assumed that the Rabi frequencies of the circular components of the input control radiation exceed the Doppler width for the quantum transition that is resonant with the probe field. The Rabi frequency of the input probe pulse was assumed to be lower than the aforementioned width by a factor of about 10. The main conclusions of our analysis can be formulated as follows.

(1) In the case of identical linear polarisations of the interacting radiations (under the condition of exact resonance for the control field), we revealed a nonmonotonic dependence of the transparency of the medium for the probe radiation of adiabaton on the detuning of its frequency from the central frequency of the corresponding quantum transition. If a medium has a sufficient length, a transmission band centred at zero resonance detuning and an absorption band adjacent to it are formed in the frequency range of the probe radiation. The presence of the transmission band is explained by the EIT phenomenon. During propagation, the probe-pulse attenuation in the range of absorption bands exceeds the attenuation that the same pulse would undergo in the absence of control radiation. This means that, at sufficiently large detunings of the probe radiation from resonance, EIT is replaced with electromagnetically induced absorption. At even larger detunings the influence of both effects on the probe-pulse evolution gradually disappears, and the transmittance monotonically increases, tending to that for nonresonant radiation. The spectral widths of the transparency window and the absorption windows for the probe radiation are of the same order of magnitude as the Doppler width of the transition that is in resonance with the probe pulse. This is explained by the choice of a high Rabi frequency of the control field in the calculations.

(2) The probe-pulse velocity in the case of exact resonance is lower than the speed of light in vacuum (by an order of magnitude under our conditions). With an increase in resonance detuning within the transparency window, it decreases by one more order of magnitude. At detunings exceeding the ones corresponding to absorption windows, the probe pulse velocity tends to the speed of light in vacuum.

(3) In the case of linearly polarised fields and exact resonance for the probe field, an increase in the resonance detuning for the control field leads to a monotonic decrease in the transmittance for the probe pulse. The probe-pulse velocity decreases under these conditions.

(4) For linearly polarised probe radiation and circularly polarised control radiation, the adiabaton probe pulse is split into two isolated pulses with oppositely directed circular polarisations. An increase in the probe-field resonance detuning leads primarily to the absorption by the medium of the probe-field component for which the circular polarisation direction coincides with the direction of the control-field circular polarisation.

References

1. Harris S.E. *Phys. Today*, **50**, 36 (1997).
2. Lukin M.D. *Rev. Mod. Phys.*, **75**, 457 (2003).
3. Duan L.-M., Lukin M.D., Cirac J.I., Zoller P. *Nature (London)*, **414**, 413 (2001).
4. Sinara A. *Phys. Rev. Lett.*, **97**, 253601 (2006).
5. Fleischhauer M., Imamoğlu A., Marangos J.P. *Rev. Mod. Phys.*, **77**, 633 (2005).
6. Martinelly M., Valente P., Failache H., Felinto D., Cruz L.S., Nussenzveig P., Lezama A. *Phys. Rev. A*, **69**, 043809 (2004).
7. Gordon A., Micalizio S., Levi F. *Phys. Rev. A*, **66**, 063807 (2002).
8. Lukin M.D., Imamoglu A. *Nature (London)*, **413**, 273 (2001).
9. Ham B.S., Hemmer P.R., Shahriar M.S. *Opt. Commun.*, **144**, 227 (1997).
10. Nikonov D.E., Imamoğlu A., Scully M.O. *Phys. Rev. B*, **59**, 12212 (1999).
11. Abdumalikov A.A. Jr., Astafiev O., Zagoskin A.M., Pashkin Yu.A., Nakamura Y., Tsai J.S. *Phys. Rev. Lett.*, **104**, 193601 (2010).
12. Tassin P., Zhang L., Koschny T., Economou E.N., Soukoulis C.M. *Opt. Express*, **17**, 5595 (2009).
13. Akulshin A.M., Barreiro S., Lezama A. *Phys. Rev. A*, **57**, 2996 (1998).
14. Lezama A., Barreiro S., Akulshin A.M. *Phys. Rev. A*, **59**, 4732 (1999).
15. Grobe R., Hioe F.T., Eberly J.H. *Phys. Rev. Lett.*, **73**, 3183 (1994).
16. Grobe R., Eberly J.H. *Laser Phys.*, **5**, 542 (1995).
17. Eberly J.H., Rahman A., Grobe R. *Laser Phys.*, **6**, 69 (1996).
18. Shakhmuratov R.N., Odeurs J. *Phys. Rev. A*, **74**, 043807 (2006).
19. Hioe F.T. *Phys. Rev. A*, **78**, 063807 (2008).
20. Oreg J., Hioe F.T., Eberly J.H. *Phys. Rev. A*, **29**, 690 (1984).
21. Kuklinski J.R., Gaubatz U., Hioe F.T., Bergmann K. *Phys. Rev. A*, **29**, 6741 (1989).
22. Kasapi A., Maneesh Jain, Yin G.Y., Harris S.E. *Phys. Rev. Lett.*, **74**, 2447 (1995).
23. DeZafra R.L., Marshall A. *Phys. Rev.*, **170**, 28 (1968).
24. Born M., Wolf E. *Principles of Optics: Electromagnetic Theory of Propagation, Interference, and Diffraction of Light* (Oxford: Pergamon, 1964; Moscow: Nauka, 1970).
25. Volkov A.V., Druzhinina N.A., Parshkov O.M. *Kvantovaya Elektron.*, **39**, 917 (2009) [*Quantum Electron.*, **39**, 917 (2009)].
26. Vol'kenshtein M.V. *Molekulyarnaya optika* (Molecular Optics) (Moscow–Leningrad: GITTL, 1951).
27. Grigor'ev I.S., Meilikhov E.Z. (Eds) *Handbook of Physical Quantities* (Boca Raton, FL: CRC Press, 1997; Moscow: Energoatomizdat, 1991).